# Temperature-independent electron tunneling injection in tris (8-hydroxyquinoline) aluminum thin film from high-work-function gold electrode

Toshinori Matsushima [a] and Chihaya Adachi [a,b,*]

[a] Core Research for Evolutional Science and Technology Program, Japan Science and Technology Agency, 1-32-12 Higashi, Shibuya, Tokyo 150-0011, Japan

[b] Center for Future Chemistry, Kyushu University, 744 Motooka, Nishi, Fukuoka 819-0395, Japan

**Abstract**

We fabricated electron-only tris (8-hydroxyquinoline) aluminum ($Alq_3$) single-layer devices with a device structure of glass substrate/MgAg anode (100 nm)/$Alq_3$ layer (100 nm)/metal cathode (100 nm), and systematically varied the work functions (*WF*) of the metal cathodes from *WF* = -1.9 (Cs) to -2.9 (Ca), -3.8 (Mg), -4.4 (Al), -4.6 (Ag), and -5.2 eV (Au) to investigate how electron injection barriers at the cathode/$Alq_3$ interfaces influence their current density-voltage (*J*-*V*) characteristics. We found that current

densities at a certain driving voltage decrease and the temperature dependence of *J-V* characteristics of the devices gradually becomes weaker as the work functions of the metal cathodes are decreased. The device with the highest-work-function Au cathode exhibited virtually temperature-independent *J-V* characteristics, suggesting that a current flow mechanism of this device is mainly controlled by electron tunneling injection at the Au/$Alq_3$ interface.

*Keywords:* tris (8-hydroxyquinoline) aluminum; organic light-emitting diode; gold electrode; current density-voltage characteristics; carrier tunneling injection; current flow mechanism

* *E-mail:* adachi@cstf.kyushu-u.ac.jp

## 1. Introduction

Organic light-emitting diodes (OLEDs) have attracted much attention recently due to their high potential for use in low-cost, large-area, lightweight, flexible displays, and other illumination applications [1]. Excellent device characteristics, such as a high external quantum efficiency of 29% [2], a high power conversion efficiency of 133 lm/W [2], a long lifetime of 1 x $10^7$ h [3], and a low driving voltage of 2.9 V at a current density of 100 mA/$cm^2$ [4], have been demonstrated in OLEDs. However, although many researchers are eager to establish the current flow mechanisms of organic thin films [5-16], their current flow mechanisms have not yet been elucidated, and must be completely clarified to bring about maximum OLED performance. A detailed understanding of the current flow mechanisms will provide a guide to further improve OLED characteristics, such as driving voltages, power conversion efficiencies, and lifetimes. Elucidation of the current flow mechanism in tris (8-hydroxyquinoline) aluminum ($Alq_3$) thin films is advantageous for development of OLEDs, and we selected $Alq_3$ as a model material to investigate current density-voltage (*J*-*V*) characteristics of $Alq_3$ thin films because $Alq_3$ is a very good electron-transport green-fluorescent material in OLEDs [17].

Carrier injection in organic layers from metal electrodes is one of the most important processes that markedly influence *J-V* characteristics of organic thin-film devices [5,8-13]. Electron injection in $Alq_3$ thin films with various electron-injecting contacts [8-11] and electron injection and transport in $Alq_3$ thin films prepared in an ultrahigh vacuum condition [12,13] have been intensively studied. However, measuring *J-V* characteristics in a wide temperature range, which is a powerful tool used to characterize current flow mechanisms of organic thin films, has not been done in previous works on $Alq_3$ thin films. In this report, we mainly discuss the temperature dependence of *J-V* characteristics of $Alq_3$ single-layer devices with various-work-function metal cathodes to better understand their current flow mechanisms.

We fabricated electron-only $Alq_3$ single-layer devices with a device structure of glass substrate/MgAg anode (100 nm)/$Alq_3$ layer (100 nm)/metal cathode (100 nm) as simplified model devices, and we systematically changed the work functions (*WF*) of the metal cathodes from *WF* = -1.9 (Cs) to -2.9 (Ca), -3.8 (Mg), -4.4 (Al), -4.6 (Ag), and -5.2 eV (Au) to investigate how electron injection barriers at the cathode/$Alq_3$ interfaces influence the temperature dependence of their *J-V* characteristics. In these devices, we

confirmed that hole currents from the MgAg anodes are negligible due to a large hole injection barrier of 1.9 eV at the MgAg/$Alq_3$ interface. We demonstrated that the temperature dependence of *J*-*V* characteristics of the electron-only $Alq_3$ devices gradually becomes weaker as electron injection barriers at the cathode/$Alq_3$ interfaces are increased. The $Alq_3$ device with the highest-work-function Au cathode exhibited virtually temperature-independent *J*-*V* characteristics, suggesting that a current flow mechanism of the $Alq_3$ device having au Au cathode is controlled by electron tunneling injection at the Au/$Alq_3$ interface.

## 2. Experimental details

The schematics of the $Alq_3$ single-layer device structures are shown in Figs. 1(a) and 1(b). Glass substrates coated with 100-nm-thick indium tin oxide (ITO) layers with a sheet resistivity of 25 Ω/sq, purchased from Sanyo Vacuum Industries Co., Ltd., were cleaned ultrasonically in detergent (Cica clean *LX*-II, Kanto Chemicals Co.)/pure water (1/10 by volume) for 10 min, followed by ultrasonication in pure water for 10 min, acetone for 10 min, and isopropanol for 10 min. After the ultrasonication, the substrates were soaked in boiling isopropanol for 5 min, and placed in an UV-$O_3$ cleaning chamber (UV.TC.NA.003, Bioforce Nanoscience, Inc.) for 30 min. Then, the cleaned substrates

were transferred to a vacuum chamber, which was evacuated to ≈ $10^{-4}$ Pa using a rotary mechanical pump and a turbo molecular pump. Organic and metal layers were successively deposited in a vacuum on the cleaned ITO surfaces at a background pressure of ≈ $10^{-4}$ Pa using resistively heated tantalum boats to fabricate the following $Alq_3$ single-layer devices with various-work-function metal anodes and a low-work-function Ca/Al cathode, i.e., glass substrate/ITO (100 nm)/*X* (5 nm)/$Alq_3$ (100 nm)/Ca (0.5 nm)/Al (100 nm), where *X* is Au, Ag, Al, MgAg, or Ca [see the device structure shown in Fig. 1(a)]. Using these devices, we investigated the influence of hole injection barriers at the metal anode/$Alq_3$ interfaces on *J*-*V* characteristics of the $Alq_3$ devices, which is discussed later in Sec. 3.1. Next, we fabricated the following electron-only $Alq_3$ single-layer devices having a low-work-function MgAg anode and various-work-function metal cathodes, i.e., glass substrate/MgAg (100 nm)/$Alq_3$ (100 nm)/*Y*, where *Y* is Au (100 nm), Ag (100 nm), Al (100 nm), MgAg (100 nm), Ca (0.5 nm)/Al (100 nm), or Cs (0.5 nm)/Al (100 nm) [see the device structure shown in Fig. 1(b)]. With these devices, we investigated the influence of electron injection barriers at the metal cathode/$Alq_3$ interfaces on *J*-*V* characteristics of the $Alq_3$ devices, which is discussed later in Sec. 3.2. To construct the above-mentioned devices, we used the evaporation rates of 0.3 nm/s for $Alq_3$, 0.1 nm/s for Al, Au, and Ag, 0.33 nm/s for MgAg

(Mg/Ag = 10/1 by weight), and 0.02 nm/s for Ca and Cs. We deposited the metal cathodes on the $Alq_3$ layers using a shadow mask to define the active area of 0.785 $mm^2$. We measured current density-voltage-luminance characteristics of the $Alq_3$ devices with a semiconductor parameter analyzer (E5250A, Agilent Technologies Inc.) and a calibrated silicon photodiode (1930-C, Newport Co.) at room temperature. The temperature dependence of *J-V* characteristics of the $Alq_3$ devices was measured in the temperature range between 350 and 200 K with a semiconductor parameter analyzer (4155C, Agilent Technologies Inc.) and a vacuum cryostat (UMC-235, Measure Jig Co., Ltd.) equipped with a Peltier cooler (R2300-7, MMR Technologies Inc.).

We assumed that the highest occupied molecular orbital (HOMO) and lowest unoccupied molecular orbital (LUMO) levels of $Alq_3$ thin films are identical with their ionization potential energies and electron affinities, respectively. To obtain the HOMO level of $Alq_3$, we prepared a 100-nm-thick $Alq_3$ layer on a cleaned glass substrate, and determined its HOMO level to be -5.7 eV by using photoelectron spectroscopy (AC-1, Riken Keiki Co., Ltd.). We calculated the LUMO level of $Alq_3$ to be -3.0 eV by subtracting the optical absorption onset energy, i.e., the energy gap (1.7 eV), from the HOMO level (-5.7 eV). The work functions of the metal electrodes were found to be

-5.2 eV for Au [5], -4.6 eV for Ag [5], -4.4 eV for Al [5], -3.8 eV for MgAg [18], -2.9 eV for Ca [5,14], and -1.9 eV for Cs [14]. The energy-level diagrams of the $Alq_3$ devices with these values are depicted in Fig. 2.

## 3. Results and discussion

### *3.1. Current density-voltage characteristics depending on work functions of metal anodes*

Here, we discuss the dependence of *J-V* characteristics of the $Alq_3$ devices on hole injection barriers at the metal anode/$Alq_3$ interfaces [the device structure is shown in Fig. 1(a)]. Low-work-function Ca (*WF* = -2.9 eV) was used as an efficient electron-injecting cathode, and the work functions of the metal anodes on the ITO electrodes were systematically changed from *WF* = -2.9 (Ca) to -3.8 (Mg), -4.4 (Al), -4.6 (Ag), and -5.2 eV (Au) [the energy-level diagram is shown in Fig. 2(a)]. The room-temperature *J-V* and external quantum efficiency-current density ($\eta_{ext}$-*J*) characteristics of the $Alq_3$ devices with the various-work-function metal anodes and the low-work-function Ca cathode are shown in Figs. 3(a) and 3(b), respectively. We measured electroluminescence of these devices from the glass substrate side through the 5-nm-thick semitransparent metal anodes.

The highest $\eta_{ext}$ was ≈ 0.03% for the device with the Au anode, and this value is about two orders of magnitude lower than that of a conventional bilayer OLED, such as glass substrate/ITO/N,N′-diphenyl-N,N′-bis(1-naphthyl)-1,1′-biphenyl-4,4′-diamine (α-NPD)/$Alq_3$/Cs/Al [the maximum $\eta_{ext}$ in this OLED was reported to be ≈ 1% in [19]. Since an electron mobility [1.4 x $10^{-6}$ $cm^2/(V \cdot s)$] is much higher than a hole mobility [2 x $10^{-8}$ $cm^2/(V \cdot s)$] in $Alq_3$ thin films [20], this low $\eta_{ext}$ is due to imbalanced recombination of electrons and holes in the $Alq_3$ layers. We suppose that the light absorption caused by the semitransparent metal anodes is a minor effect for the low $\eta_{ext}$.

As can be seen in Figs. 3(a) and 3(b), the *J*-*V* curves gradually shifted to higher current densities and $\eta_{ext}$ increased as the work functions of the metal anodes were decreased from *WF* = -2.9 (Ca) to -3.8 (Mg), -4.4 (Al), -4.6 (Ag), and -5.2 eV (Au). In general, it is possible that two-carrier injection of electrons and holes provides higher current densities than single-carrier injection of either electrons or holes because space-charge fields induced by injected electrons and holes neutralize each other in organic layers [21]. Therefore, we attribute the gradual shift of the *J*-*V* curves to higher current densities to enhanced hole injection in the $Alq_3$ layers due to lowered hole

injection barriers at the anode/$Alq_3$ interfaces. Moreover, the *J-V* curves of the $Alq_3$ devices with the MgAg and Ca anodes were almost identical and no electroluminescence was observed from these devices, indicating completely unipolar electron injection in the $Alq_3$ layers.

### *3.2. Current density-voltage characteristics depending on work functions of metal cathodes*

In this section, we discuss the dependence of *J-V* characteristics of the electron-only $Alq_3$ single-layer devices on electron injection barriers at the cathode/$Alq_3$ interfaces [the device structure is shown in Fig. 1(b)]. Low-work-function MgAg (*WF* = -3.8 eV) was used as an anode to prevent hole injection, as was discussed in Sec. 3.1, and the work functions of the metal cathodes were systematically changed from *WF* = -1.9 (Cs) to -2.9 (Ca), -3.8 (Mg), -4.4 (Al), -4.6 (Ag), and -5.2 eV (Au) [the energy-level diagram is shown in Fig. 2(b)]. The room-temperature *J-V* characteristics of the electron-only $Alq_3$ devices having the low-work-function MgAg anode and the various-work-function metal cathodes are shown in Fig. 4.

The *J-V* curves of the electron-only $Alq_3$ devices shifted to higher current densities as

the work functions of the metal cathodes were increased from *WF* = -5.2 to -3.8 eV, and the *J-V* curves became almost unchanged when we used the work functions of *WF* = -3.8 (Mg), -2.9 (Ca), and -1.9 eV (Cs). Since Stöβel *et al*. reported that low-work-function metals are easily oxidized during the metal depositions under a high vacuum condition of ≈ $10^{-4}$ Pa [11], we speculate that the slight oxidation of Mg, Ca, and Cs occurs near the electrode/$Alq_3$ interfaces during the depositions and the formation of the thin metal oxide layers lowers an electron injection efficiency at the interfaces and results in the unchanged *J-V* characteristics. Furthermore, it is noteworthy that electrons can be injected in the $Alq_3$ layer from the high-work-function Au cathode across a large electron injection barrier of 2.2 eV. However, it should be noted that an actual electron injection barrier would become smaller than 2.2 eV due to a vacuum level shift at organic/metal heterojunction interfaces [22]. A carrier injection mechanism at this Au/$Alq_3$ interface is discussed later in Sec. 3.3.

We investigated the temperature dependence of *J-V* characteristics of the electron-only $Alq_3$ single-layer devices discussed above. The temperature dependence of the *J-V* characteristics of the $Alq_3$ devices in the temperature range between 350 and 200 K is shown in Fig. 5. From these figures, one can see that the $Alq_3$ devices with the

lower-work-function Cs (*WF* = -1.9 eV), Ca (*WF* = -2.9 eV), and MgAg (*WF* = -3.8) cathodes exhibited stronger temperature dependence of the *J*-*V* characteristics [Figs. 5(a), 5(b), and 5(c)], while the temperature dependence of the *J*-*V* characteristics gradually became weaker as the work functions of the metal cathodes were decreased from -3.8 (Mg) to -4.4 (Al), -4.6 (Ag), and -5.2 eV (Au) [Figs. 5(c), 5(d), 5(e), and 5(f)]. In particular, the *J*-*V* characteristics of the $Alq_3$ device with the Au cathode were almost temperature independent.

When an ohmic contact is formed between metallic electrodes and organic films, *J*-*V* characteristics are controlled by transport-limited currents. The well-established trapped-charge-limited current conduction with an exponential trap distribution [21] is given by the equation,

$$J = N_c \mu e^{(1-l)} \left[ \frac{\varepsilon_r \varepsilon_0 l}{N_t (l+1)} \right]^l \left( \frac{2l+1}{l+1} \right)^{(l+1)} \frac{V^{(l+1)}}{L^{(2l+1)}} \quad \text{and} \quad l = \frac{T_t}{T}, \tag{1}$$

where $N_v$ is the effective density of states in the conduction band, $\mu$ is the electron mobility, $N_t$ is the electron trap concentration, $\varepsilon_r$ is relative permittivity, $\varepsilon_0$ is the vacuum permittivity, $L$ is the cathode-anode spacing in a planar geometry, $T$ is the temperature, and $T_t$ is the characteristic temperature of an exponential trap distribution. When an electron injection barrier between metallic electrodes and organic films is relatively

large, on the other hand, *J-V* characteristics are controlled by injection-limited currents. The promising injection-limited current model is a Fowler-Nordheim carrier tunneling injection current [5,23], which is given by the equation,

$$J \propto \frac{F^2}{\Phi} \exp\left( -\frac{8(2m^*)^{0.5}\Phi^{1.5}}{3hqF} \right), \quad (2)$$

where $\Phi$ is the metal-insulator barrier height, $F$ is the electric field, $h$ is the Plank's constant, $q$ is the electronic charge, and $m$ is the effective mass of carriers in a solid. Generally, thermally activated carrier transport currents, such as Eq. (1), are temperature dependent. On the contrary, carrier tunneling injection currents, such as Eq. (2), are temperature independent. Based on these carrier transport and injection models, we speculate that current flow mechanisms of the $Alq_3$ devices are gradually changed from a temperature-dependent thermally activated electron transport mechanism to a temperature-independent electron tunneling injection mechanism as the electron injection barriers at the cathode/$Alq_3$ interfaces are increased.

### *3.3. Detailed investigation of electron injection in $Alq_3$ layers*

To obtain more detailed information on an electron injection mechanism at the Au/$Alq_3$ interface, we compared *J-V* characteristics obtained in two kinds of $Alq_3$ single-layer devices sandwiched with Au and MgAg electrodes:

glass substrate/MgAg (100 nm)/$Alq_3$ (100 nm)/Au (100 nm) [device (A)]

and glass substrate/Au (100 nm)/$Alq_3$ (100 nm)/MgAg (100 nm) [device (B)].

These devices were operated in both forward and reverse bias directions. In the forward bias, the Au and MgAg electrodes were wired as an anode and a cathode, respectively. The room-temperature *J-V* characteristics of the forward and reverse biased $Alq_3$ devices (A) and (B) are shown in Fig. 6.

When these devices were forward biased, small carrier injection barriers at the MgAg/$Alq_3$ and Au/$Alq_3$ interfaces provided two-carrier injection of electrons and holes into the $Alq_3$ layers. However, although the configurations of these devices (A) and (B) were simply inverted, current densities of the forward biased device (B) were higher than those of the forward biased device (A). Moreover, while the rectilinear *J-V* curve was clearly observed in the reverse biased device (A), the reverse biased device (B) exhibited much lower current densities than those of the reverse biased device (A).

Kiy *et al*. fabricated $Alq_3$ single-layer devices sandwiched with symmetric Mg electrodes and reported that *J-V* curves of their devices do not depend on the electron injection directions [12], which is inconsistent with our results mentioned above. In this

study, we used MgAg alloy electrodes instead of pure Mg electrodes to prevent the oxidization of Mg and to improve a sticking coefficient of Mg on organic surfaces [17]. Therefore, preparing MgAg on the $Alq_3$ thin films would improve a sticking coefficient of Mg on the $Alq_3$ surfaces and an electron injection efficiency at these interfaces. Since the melting temperature of Au (1064ºC) is higher than those of Ag (961ºC) and Mg (650ºC), depositing the hotter Au electrode on the $Alq_3$ layer may improve the sticking coefficient and the electron injection efficiency at the Au/$Alq_3$ interface.

To better understand the difference of electron injection characteristics of these devices, we measured the temperature dependence of the *J-V* characteristics of the forward and reverse biased device (A) in the temperature range between 350 and 200K, and the results are shown in Fig. 7. Small electron and hole injection barriers at the MgAg/$Alq_3$ and Au/$Alq_3$ interfaces in the forward biased device (A) provided two-carrier injection of electrons and holes and temperature-dependent *J-V* characteristics. On the contrary, the reverse biased device (A) had temperature-independent *J-V* characteristics controlled by electron tunneling injection from the Au cathode.

Finally, we mention the weakness of our argument. Although we tried fitting the *J*-*V* characteristics with the trapped-charge-limited current model, which is given by Eq. (1), and the Fowler-Nordheim carrier tunneling injection current model, which is given by Eq. (2), we were unsuccessful in fitting the experimental data with these models with reasonable fitting parameters, indicating that some current flow mechanism in organic thin-film devices remains unknown. We are now striving to understand this current flow mechanism.

## 4. Conclusion

We investigated *J*-*V* and $\eta_{ext}$-*J* characteristics of $Alq_3$ single-layer devices sandwiched with a low-work-function Ca cathode and various-work-function metal anodes. We confirmed that virtually no hole injection occurs in the devices with lower-work-function MgAg and Ca anodes. Furthermore, we investigated *J*-*V* characteristics of electron-only $Alq_3$ single-layer devices sandwiched with a low-work-function MgAg anode and various-work-function metal cathodes. We demonstrated that the smaller electron injection barriers between metal cathodes and $Alq_3$ layers enhance electron injection efficiencies, and the temperature dependence of *J*-*V* characteristics gradually becomes weaker as electron injection barriers are increased

in these devices. In particular, *J-V* characteristics of the device with the Au cathode were almost temperature independent. From these results, we concluded that current flow mechanisms of the electron-only $Alq_3$ devices were gradually changed from a temperature-dependent thermally activated electron transport process to a temperature-independent electron tunneling injection process as the electron injection barriers were increased.

**References**

[1] S. R. Forrest, Nature (London) 428 (2004) 911.

[2] D. Tanaka, H. Sasabe, Y.-J. Li, S.-J. Su, T. Takeda, J. Kido, Jpn. J. Appl. Phys. 46 (2007) 10.

[3] R. Meerheim, K. Walzer, M. Pfeiffer, K. Leo, Appl. Phys. Lett. 89 (2006) 061111.

[4] T. Matsushima, C. Adachi, Appl. Phys. Lett. 89 (2006) 253506.

[5] I. D. Parker, J. Appl. Phys. 75 (1994) 1656.

[6] P. E. Burrows, Z. Shen, V. Bulovic, D. M. McCarty, S. R. Forrest, J. A. Cronin, M. E. Thompson, J. Appl. Phys. 79 (1996) 7991.

[7] S. Barth, U. Wolf, H. Bässler, P. Müller, H. Riel, H. Vestweber, P. F. Seidler, W. Rieβ, J. Appl. Phys. 60 (1999) 8791.

[8] M. Stöβel, J. Staudigel, F. Steuber, J. Simmerer, G. Wittmann, A. Kanitz, H. Klausmann, W. Rogler, W. Roth, J. Schumann, A. Winnacker, Phys. Chem. Chem. Phys. 1 (1999) 1791.

[9] M. Stöβel, J. Staudigel, F. Steuber, J. Simmerer, A. Winnacker, Appl. Phys. A 68 (1999) 387.

[10] M. Stöβel, J. Staudigel, F. Steuber, J. Blässing, J. Simmerer, Appl. Phys. Lett. 76 (2000) 115.

[11] M. Stöβel, J. Staudigel, F. Steuber, J. Blässing, J. Simmerer, A. Winnacker, H. Neuner, D. Metzdorf, H.-H. Johannes, W. Kowalsky, Synth. Metals 111 (2000) 19.

[12] M. Kiy, I. Biaggio, M. Koehler, P. Günter, Appl. Phys. Lett. 80 (2002) 4366.

[13] M. Kiy, P. Losio, I. Biaggio, M. Koehler, A. Tapponnier, P. Günter, Appl. Phys. Lett. 80 (2002) 1198.

[14] T. Oyamada, C. Maeda, H. Sasabe, C. Adachi, Jpn. J. Appl. Phys. 42 (2003) 1535.

[15] T. Matsushima, C. Adachi, Appl. Phys. Lett. 88 (2006) 033508.

[16] T. Matsushima, K. Goushi, C. Adachi, Chem. Phys. Lett. 435 (2007) 327.

[17] C. W. Tang, S. A. VanSlyke, Appl. Phys. Lett. 51 (1987) 913.

[18] The work function of MgAg was measured to be - 3.8 eV using AC-1.

[19] T. Oyamada, H. Sasabe, C. Adachi, S. Murase, T. Tominaga, C. Maeda, Appl. Phys. Lett. 86 (2005) 033503.

[20] R. G. Kepler, P. M. Beeson, S. J. Jacobs, R. A. Anderson, M. B. Sinclair, V. S. Valencia, P. A. Cahill, Appl. Phys. Lett. 66 (1995) 3618.

[21] M. A. Lampert, P. Mark, Current Injection In Solids (ACADEMIC, New York, 1970).

[22] S. T. Lee, X. Y. Hou, M. G. Mason, C. W. Tang, Appl. Phys. Lett. 72 (1998) 1593.

[23] R. H. Fowler, L. Nordheim, Proc. R. Soc. London Ser. A 119 (1928) 173.

**Figure captions**

Fig. 1. Device structure schematics of (a) $Alq_3$ devices with low-work-function Ca cathode and various-work-function metal anodes and (b) electron-only $Alq_3$ devices with low-work-function MgAg anode and various-work-function metal cathodes.

Fig. 2. Energy-level diagrams of (a) $Alq_3$ devices with low-work-function Ca cathode and various-work-function metal anodes and (b) electron-only $Alq_3$ devices with low-work-function MgAg anode and various-work-function metal cathodes. In these figures, lowest unoccupied molecular orbital and highest occupied molecular orbital levels of $Alq_3$ are abbreviated as LUMO and HOMO levels, respectively.

Fig. 3. (a) Room-temperature current density-voltage and (b) external quantum efficiency-current density characteristics of $Alq_3$ single-layer devices with low-work-function Ca cathode and various-work-function metal anodes.

Fig. 4. Room-temperature current density-voltage characteristics of electron-only $Alq_3$ single-layer devices with low-work-function MgAg anode and various-work-function metal cathodes.

Fig. 5. Temperature dependence of current density-voltage characteristics of electron-only $Alq_3$ single-layer devices in temperature range between 350 and 200 K. (a) Glass substrate/MgAg anode/$Alq_3$ layer/Cs cathode/Al layer, (b) glass substrate/MgAg anode/$Alq_3$ layer/Ca cathode/Al layer, (c) glass substrate/MgAg anode/$Alq_3$ layer/MgAg cathode, (d) glass substrate/MgAg anode/$Alq_3$ layer/Al cathode, (e) glass substrate/MgAg anode/$Alq_3$ layer/Ag cathode, and (f) glass substrate/MgAg anode/$Alq_3$ layer/Au cathode.

Fig. 6. Room-temperature current density-voltage characteristics of forward biased and reverse biased $Alq_3$ single-layer devices with MgAg and Au electrodes. Device structures (A) and (B) are glass substrate/MgAg/$Alq_3$/Au and glass substrate/Au/$Alq_3$/MgAg, respectively. In forward bias, Au and MgAg electrodes were wired as anode and cathode, respectively.

Fig. 7. Temperature dependence of current density-voltage characteristics of $Alq_3$ single-layer device (A) with MgAg and Au electrodes in temperature range between 350 and 200 K. In forward bias, Au and MgAg electrodes were wired as anode and cathode,

respectively. Although forward biased device (A) exhibits strong temperature dependence of current density-voltage characteristics, current density-voltage characteristics of reverse biased device (A) are almost temperature independent.

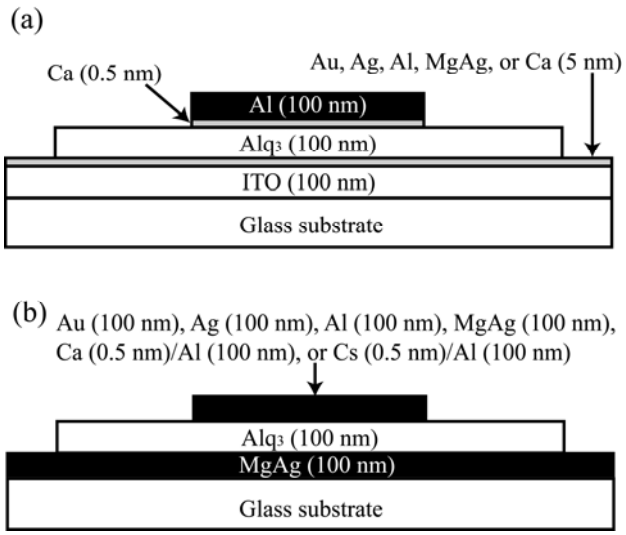


Fig. 1

T. Matsushima and C. Adachi

*Thin Solid Films*

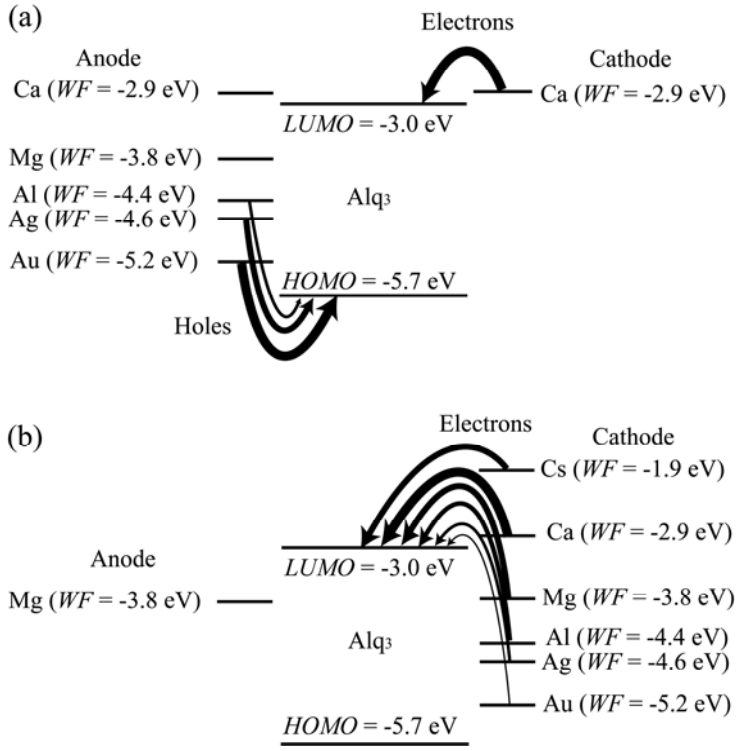


Fig. 2

T. Matsushima and C. Adachi

*Thin Solid Films*

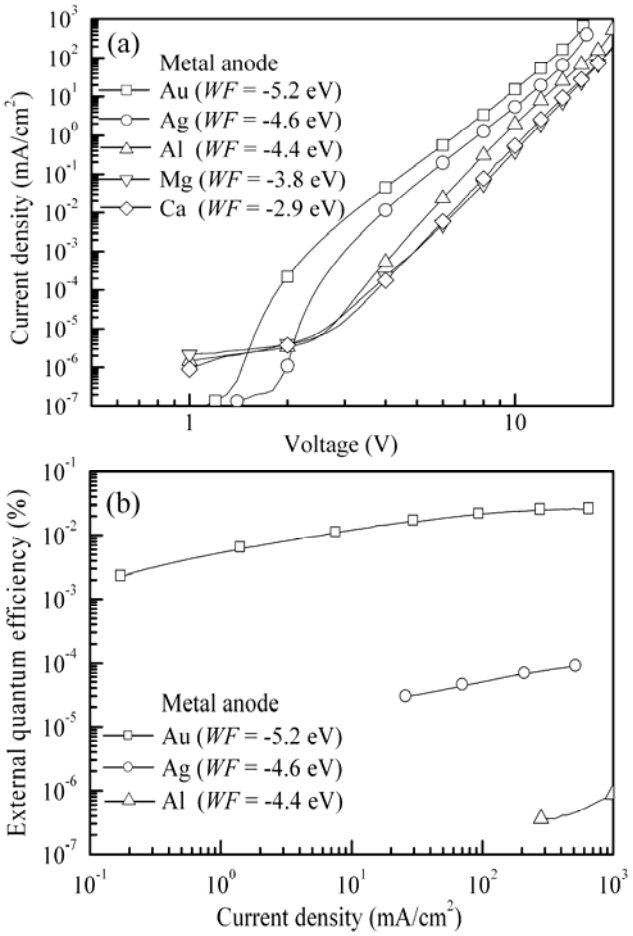


Fig. 3

T. Matsushima and C. Adachi

*Thin Solid Films*

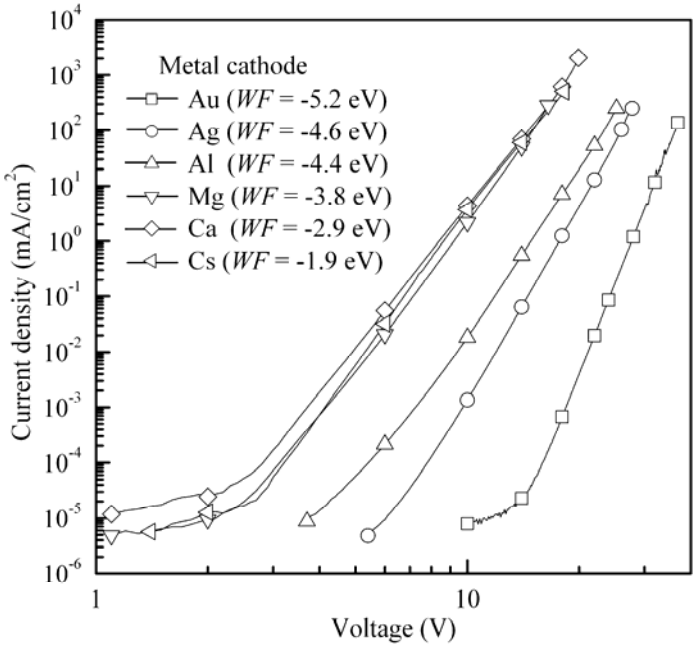


Fig. 4

T. Matsushima and C. Adachi

*Thin Solid Films*

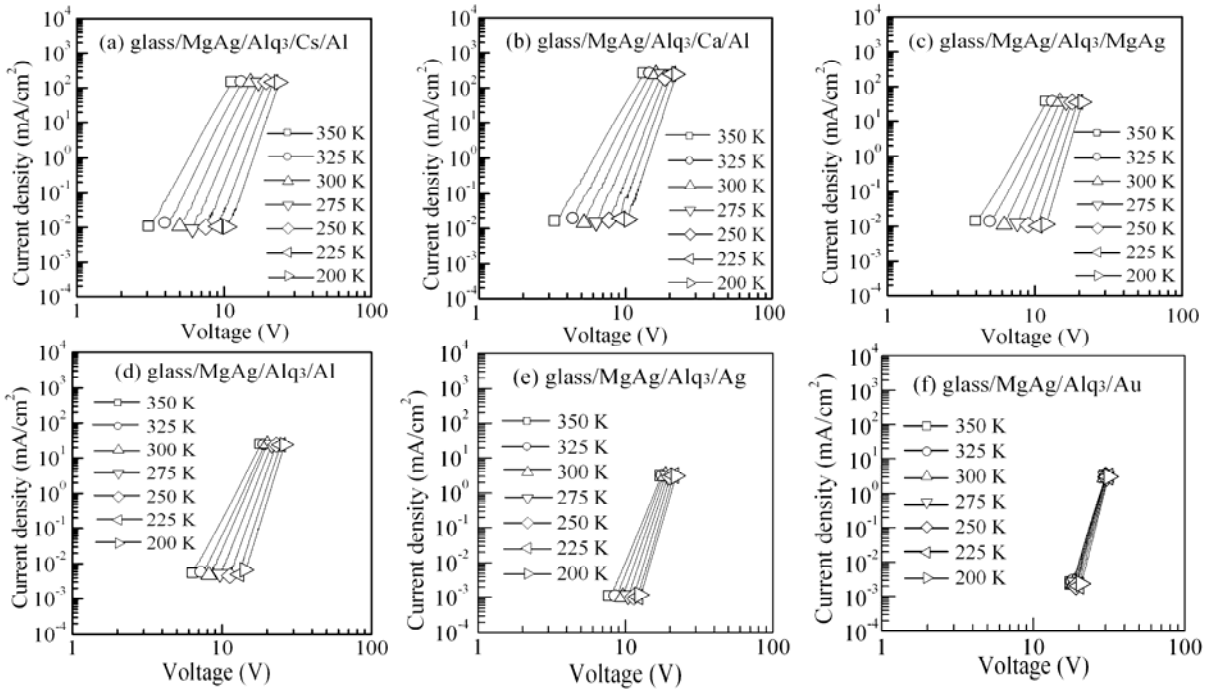


Fig. 5

T. Matsushima and C. Adachi

*Thin Solid Films*

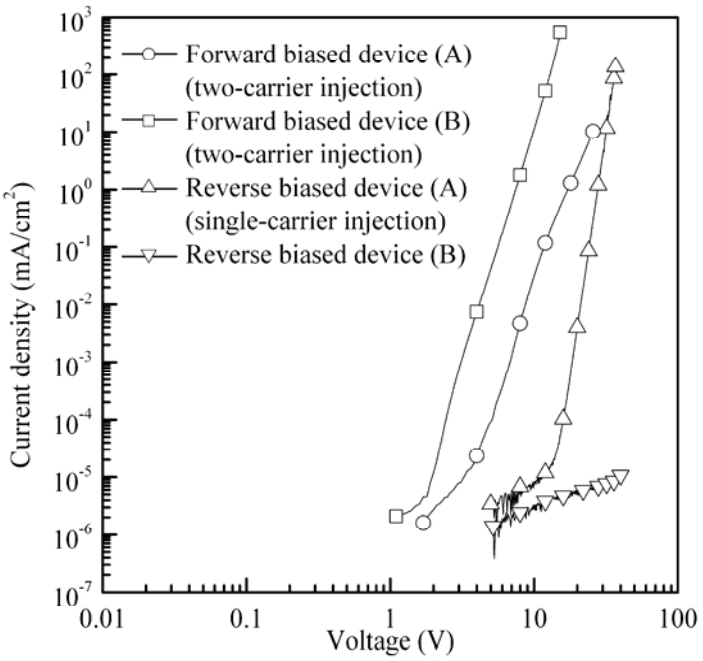


Fig. 6

T. Matsushima and C. Adachi

*Thin Solid Films*

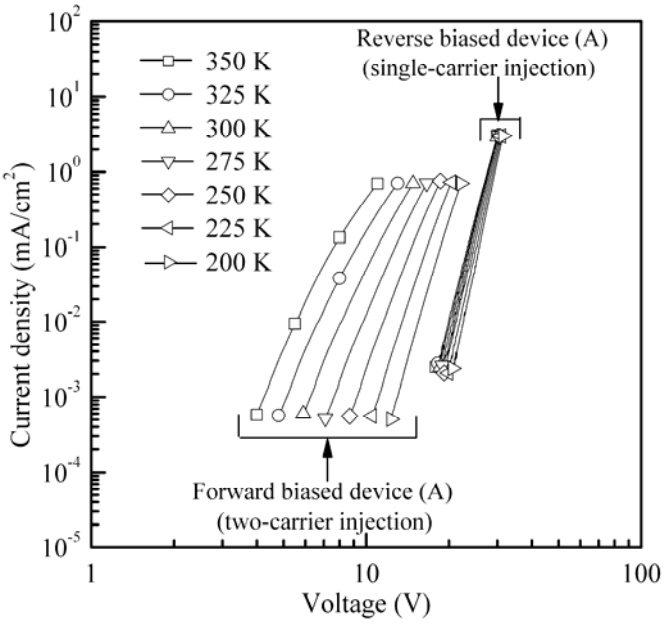


Fig. 7

T. Matsushima and C. Adachi

*Thin Solid Films*